2023 IEEE International Conference on Robotics and Automation (ICRA 2023)
May 29 - June 2, 2023. London, UK

Input-Output Boundedness of a Magnetically-Actuated Helical Device

Leendert-Jan W. Ligtenberg and Islam S. M. Khalil

***Abstract*— To date, all previous research in the wireless magnetic actuation of untethered helical devices has achieved motion stability using feedback control *in vitro*. However, feedback control systems are likely to be affected by the increased sensory uncertainty during *in vivo* trials. In this study we investigate the input-output boundedness of an interconnection between a helical device and a single rotating magnet actuator in low-Reynolds-number regime. Using the resistive-force theory, the interconnection is expressed in terms of all possible input-output pairs. Inputs representing the actuation frequency, pitch angle, lateral speed, and field strength are analyzed numerically and experimentally. We demonstrate input-output boundedness of the states of the helical device during circular and straight runs in open-loop, and we demonstrate bounded input-output propulsion without orienting the angle of attack (the often used input to swim horizontally without vertical drift) of the helical device to counteract gravity. Our results are important for a number of minimally invasive applications and tasks requiring improved control authority for stable runs of helical devices without drift due to gravity and without feedback control and restricted configuration imposed on the helical device's motion.**

I. INTRODUCTION

Untethered helical magnetic devices (UHMDs) can be used for a wide number of minimally invasive applications in medicine [1]. The range of possibilities is so vast that it is possible to use them in targeted therapy such as drugs delivery, brachytherapy, and hyperthermia, to material removal interventions such as ablation, biopsy, and thrombus fragmentation. These UHMDs have a wide variety of solutions for other biomedical applications such as steering of controllable structures (i.e., routing a stent) and sensing [2], [3]. It is often the case that the UHMD's orientation (i.e., angle of attack) is restricted during propulsion to move without drift due to gravity [4], [5], thus increasing the complexity of the design of a reliable control system. It is also often desirable to swim with a small angle of attack during transitions into Newtonian–viscoelastic interfaces and inside confinements [6]. Therefore, to achieve propulsion without extra restrictions on the angle of attack, the boundedness of UHMD's output needs to be modeled and understood.

Swimming of UHMDs in low-Reynolds-number regime has been achieved using a variety of actuation techniques, in which the long axis of the UHMD is oriented controllably based on a prescribed trajectory while simultaneously rotating to produce thrust [7], [8]. Rotating magnetic fields are generated using a single actuator or multiple actuators (i.e., permanent magnet or electromagnetic coil) [9], [10], such that the field rotation axis is controlled based on the desired motion. It has been shown that a single rotating permanent magnet (RPM) can control UHMDs while following trajectories independent of the UHMDs themselves [11]. This approach allows for direct construction of any desired magnetic field rotation axis using a unique rotation axis of the RPM, resulting in at least three important features with direct implication for locomotion. First, it allows the RPM to move freely in the workspace and avoid obstacles during actuation (Fig. 1(a)). Second, it enables the field source to employ a desirable magnetic force to assist actuation. It is possible to apply a desirable attractive magnetic force by employing multiple RPMs and create a more uniform field than a single RPM (Fig. 1(b)). An advantage of the actuation using a single RPM over multiple actuators is its ability to move freely in a relatively large workspace so long as the propulsive force of the UHMD is greater than

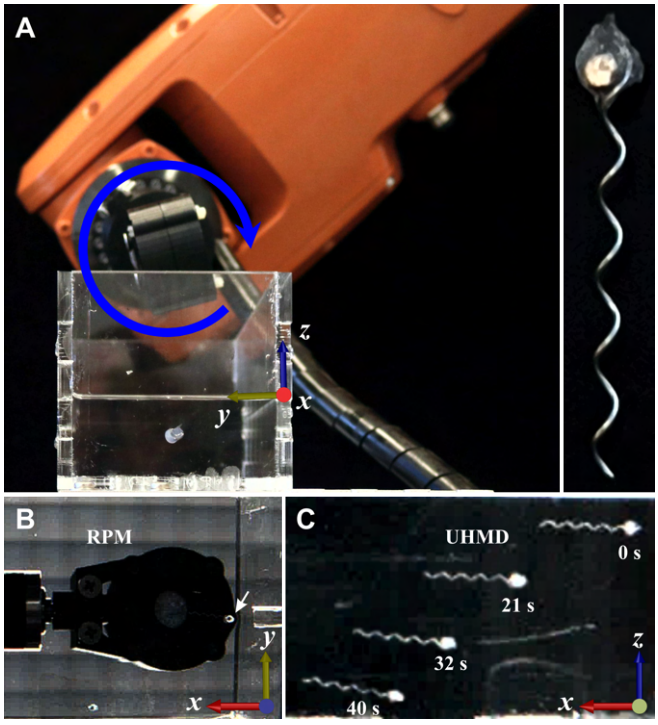

Fig. 1. Without controlling the angle of attack between the x-axis of a frame of reference and the long axis of the untethered helical magnetic device (UHMD) to compensate its own weight, it will fall downward (along the z-axis). Stable input-output pairs for the interconnection between the rotating permanent magnet (RPM) actuator and the UHMD yield swimming in straight runs with the long axis of the UHMD approximately parallel to the x-axis. (A), (B) A UHMD is actuated with a single RPM fixed to a robotic manipulator. (C) The UHMD falls along the z-axis under its own weight as it moves through the fluid along the x-axis.

The authors are with the Department of Biomechanical Engineering, University of Twente, 7500 AE Enschede, The Netherlands (e-mail: l.w.ligtenberg@student.utwente.nl, i.s.m.khalil@utwente.nl).

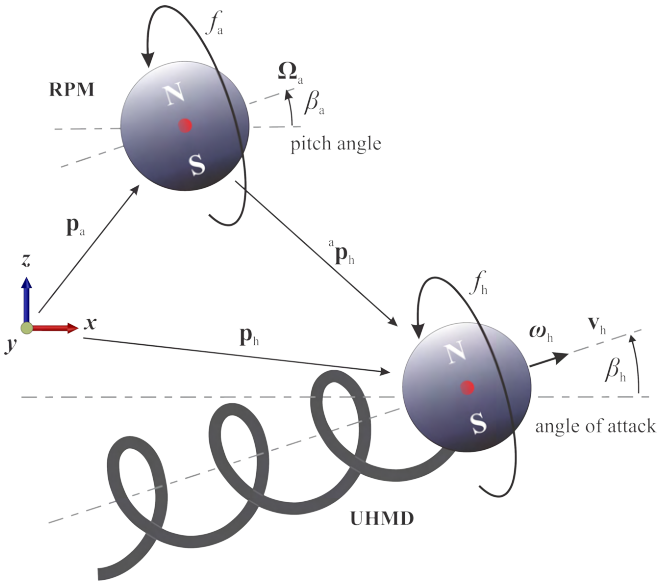

Fig. 2. An untethered helical magnetic device (UHMD) and a rotating permanent magnet (RPM) are characterized by the position vectors $\mathbf{p}_\mathrm{h}$ and $\mathbf{p}_\mathrm{a}$ with respect to a frame of reference $\{\boldsymbol{x}, \boldsymbol{y}, \boldsymbol{z}\}$, respectively. The UHMD's rotation axis, ω_h, depends on the RPM's rotation axis, $\boldsymbol{\Omega}_\mathrm{a}$. Below a step-out frequency, the UHMD rotates at f_h in sync with f_a of the RPM.

the attractive force. This is most easily achieved through the use of feedback control where the pitch angle of the RPM is determined as a function of the UHMD's angle of attack (Fig. 1(c)). However, in cases where this angle cannot be accurately measured due to sensory uncertainty or low contrast to noise ratio and low-contrast resolution [12]-[16], we need a way to quantify the boundedness of the UHMD's outputs in terms of a set of possible RPM's inputs.

In this paper, the input-output boundedness of a UHMD is investigated numerically using a 6-degrees-of-freedom (DOF) model to predict the motion of the UHMD, given the RPM's inputs. The effect of each input (frequency, pitch angle, field strength, and lateral speed) is quantified by their gain. Experimentally, the RPM's inputs are controlled robotically to study the input-output boundedness of the UHMD. Our experiments show helical propulsion with any arbitrary angle of attack with no restriction to counteract gravity.

II. Input-Output Boundedness

The motion of UHMDs can remain bounded so long as they propel themselves while gravitational and attractive forces are self-compensated. In what follows, we discuss a 6-DOF hydrodynamic model to show how to generate a bounded response through dynamic self-compensation.

A. Modeling of the Magnetically-Actuated Helical Device

We consider a UHMD actuated by an RPM, as shown in Fig. 2. The RPM is placed at $\mathbf{p}_\mathrm{a} \in \mathbb{R}^{3\times1}$ with respect to a frame of reference, and actuated at frequency f_a about the rotation axis $\hat{\boldsymbol{\Omega}}_\mathrm{a} \in \mathbb{R}^{3\times1}$ (The symbol $\hat{}$ denotes unit-length vector). The RPM has a pitch angle β_a, which controls its rotation axis, $\hat{\boldsymbol{\Omega}}_\mathrm{a}$, with respect to the $\boldsymbol{x}$-axis. The UHMD is characterized by ${}^\mathrm{a}\mathbf{p}_\mathrm{h} = [{}^\mathrm{a}p_{\mathrm{h}_x}, {}^\mathrm{a}p_{\mathrm{h}_y}, {}^\mathrm{a}p_{\mathrm{h}_z}]^T$. The actuation causes the UHMD to rotate at a frequency f_h about its rotation axis $\hat{\boldsymbol{\omega}}_\mathrm{h} \in \mathbb{R}^{3\times1}$. This axis has an angle of attack, β_h, with respect to the $\boldsymbol{x}$-axis. Rotation of a UHMD at low-Re produces translational motion at velocity $\mathbf{v}_\mathrm{h} \in \mathbb{R}^{3\times1}$. Motion of the RPM with respect to the UHMD reduces the change in the position vector ${}^\mathrm{a}\mathbf{p}_\mathrm{h}$, which enables controlling the UHMD. The pose of the RPM is given by

$$\mathbf{p}_\mathrm{a}(t) = \mathbf{R}_\mathrm{a}(\beta_\mathrm{a}, \dot{\gamma}_\mathrm{a}, t)\mathbf{p}_\mathrm{a}(t_0) + \mathbf{v}_\mathrm{a}t, \quad (1)$$

$$\hat{\boldsymbol{\Omega}}_\mathrm{a}(t) = \mathbf{R}_\mathrm{a}(\beta_\mathrm{a}, \dot{\gamma}_\mathrm{a}, t)\hat{\boldsymbol{\Omega}}_\mathrm{a}(t_0), \quad (2)$$

where $\mathbf{R}_\mathrm{a}(\beta, \dot{\gamma}, t) \in \mathbb{R}^{3\times3}$ is the following rotation matrix:

$$\mathbf{R}_\mathrm{a}(\beta_\mathrm{a}, \dot{\gamma}_\mathrm{a}, t) = \mathbf{R}_z(\dot{\gamma}_\mathrm{a}t)\mathbf{R}_y(-\beta_\mathrm{a}). \quad (3)$$

With $\mathbf{p}_\mathrm{a}$ and $\hat{\boldsymbol{\Omega}}_\mathrm{a}$ obtained from a given task space variables (i.e., β_a and γ_a), the magnetic force and torque can be determined and entered into the following force and torque balance which governs the response of the UHMD:

$$\begin{pmatrix} (\mathbf{m}_\mathrm{h} \cdot \nabla)\mathbf{B}({}^\mathrm{a}\mathbf{p}_\mathrm{h}) + \mathbf{f}_\mathrm{visc} + \mathbf{f}_\mathrm{g} \\ \mathbf{m}_\mathrm{h} \times \mathbf{B}({}^\mathrm{a}\mathbf{p}_\mathrm{h}) + \boldsymbol{\tau}_\mathrm{visc} + \boldsymbol{\tau}_\mathrm{g} \end{pmatrix} = 0, \quad (4)$$

where $\mathbf{f}_\mathrm{visc}$ and $\mathbf{f}_\mathrm{g}$ are the drag force and force due to gravity, respectively. Further, $\boldsymbol{\tau}_\mathrm{visc}$ and $\boldsymbol{\tau}_\mathrm{g}$ are their corresponding torques (see Appendix A). To demonstrate self-compensation capability through the RPM's input, Equation (4) is solved in cases where dynamic self-compensation of the gravitational and attractive forces is accomplished. Three sets of bounded inputs are provided and boundedness is investigated. The response of the UHMD in Figs. 3(a) and 3(b) can be expected and we observe attraction toward the RPM and falling downward, respectively. In the first case, the magnetic forces are much stronger than gravitational forces that are not compensated by a thrust component (Fig. 3(a)), while in the second case the attractive force is weaker than the gravitational force owing to the RPM-UHMD-gap, resulting in a falling mass. In contrast, Fig. 3(c) shows that there exists a set of bounded inputs that enables propulsion with bounded outputs, that is, the trajectories can stay identically in the same region for all future time [17].

B. Input-Output Gain

To investigate the input-output boundedness of the UHMD, input-output gain, γ, is defined and we have [18]:

$$u := {}^\mathrm{a}p_{\mathrm{h}_z}(t_0), \quad y := \min({}^\mathrm{a}p_{\mathrm{h}_z}(t)) - \max({}^\mathrm{a}p_{\mathrm{h}_z}(t)), \quad (5)$$

where y is a dependent output on the input u. The input is defined as the initial distance between the RPM and the UHMD, ${}^\mathrm{a}\mathbf{p}_\mathrm{h}$, along the $\boldsymbol{z}$-axis. The output is the difference between the minimum and maximum ${}^\mathrm{a}\mathbf{p}_{\mathrm{h}_z}(t)$ of the UHMD's trajectory, and we have the following input-output gain:

$$\gamma := \frac{\min({}^\mathrm{a}p_{\mathrm{h}_z}(t)) - \max({}^\mathrm{a}p_{\mathrm{h}_z}(t))}{{}^\mathrm{a}p_{\mathrm{h}_z}(t_0)}. \quad (6)$$

Note that $\gamma > 1$ signifies that the distance travelled by the UHMD along the $\boldsymbol{z}$-axis is greater than the initial distance with the RPM (i.e., ${}^\mathrm{a}p_{\mathrm{h}_z}(t_0)$), suggesting that the output is unbounded. In contrast, if $0 < \gamma < 1$, then the UHMD would stay between the mentioned boundary. To calculate γ, ${}^\mathrm{a}p_{\mathrm{h}_z}(t)$

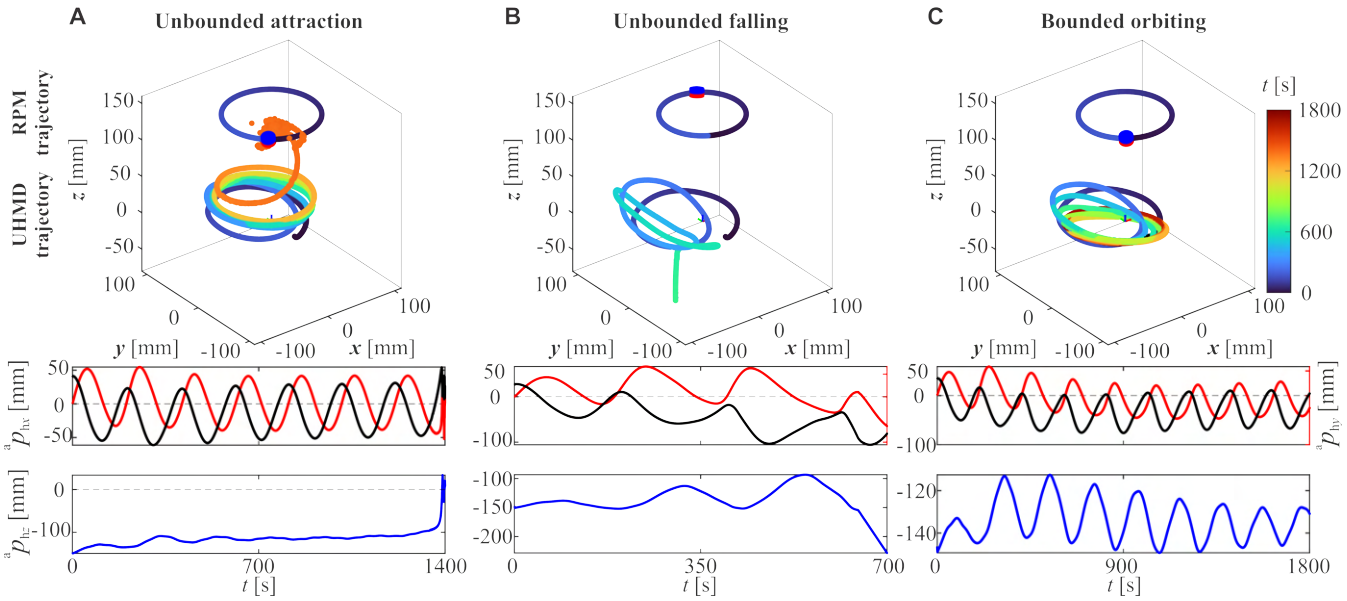

Fig. 3. The trajectories of an untethered helical magnetic device (UHMD) are calculated for three different sets of inputs. The RPM is controlled to move along a circular trajectory in the $\boldsymbol{xy}$-plane. (A) The UHMD is attracted toward the RPM for the inputs $f_\mathrm{a} = 3.3$ Hz, $|{}^\mathrm{a}\mathbf{p}_\mathrm{h}(t_0)| = 152$ mm, $\beta_\mathrm{a} = 15$ °, and $\dot{\gamma}_\mathrm{a} = 1.8$ °/s. (B) A falling UHMD for the inputs $f_\mathrm{a} = 3.3$ Hz, $|{}^\mathrm{a}\mathbf{p}_\mathrm{h}(t_0)| = 150$ mm, $\beta_\mathrm{a} = 10°$, $\dot{\gamma}_\mathrm{a} = 1.8°$/s. (C) The outputs of the UHMD remains bounded for all future time for the inputs $f_\mathrm{a} = 3.3$ Hz, $|{}^\mathrm{a}\mathbf{p}_\mathrm{h}(t_0)| = 150$ mm, $\beta_\mathrm{a} = 12.7°$, $\dot{\gamma}_\mathrm{a} = 1.8°$/s. *Please see supplementary multimedia.*

must be calculated for all time. Substituting $\mathbf{v}_\mathrm{a} = 0$ into Equation (1) results in a circular path, which is used as the desired RPM position trajectory. The inputs β_a, $|{}^\mathrm{a}\mathbf{p}_\mathrm{h}(t_0)|$ and $\dot{\gamma}_\mathrm{a}$ are varied to test the input-output boundedness. Fig. 3(a) shows the result of a radially actuated RPM with an initial distance to the UHMD, $|{}^\mathrm{a}\mathbf{p}_\mathrm{h}(t_0)| = 152$ mm, $\beta_\mathrm{a} = 15°$, and a rotational speed along the $\boldsymbol{z}$-axis $\dot{\gamma}_\mathrm{a} = 1.8°$/s. The UHMD is positioned at $\mathbf{p}_\mathrm{h}(t_0) = [0, -45, 0]^T$ mm, with zero initial pitch angle, $\beta_\mathrm{a} = 0°$. The simulation time is set at 1800 s to show if the UHMD can have bounded outputs for long period of time. However, at ~ 1300 s the UHMD is attracted toward the RPM. This results in $\gamma = 1.247$ for $t = 1400$ s, and its path becomes undetermined owing to the unbounded output.

Changing the input of the RPM to $|{}^\mathrm{a}\mathbf{p}_\mathrm{h}(t_0)| = 150$ mm, $\beta_\mathrm{a} = 10°$, and $\dot{\gamma}_\mathrm{a} = 1.8°$/s, results in the trajectories shown in Fig. 3(b). For $t > 650$ s the RPM-UHMD-gap becomes too large and the UHMD falls downward under its own weight. The resulting gain after $t = 700$ s is $\gamma = 0.914$. The trajectory of the falling UHMD indicates that the RPM is no longer able to pull the UHMD, meaning that the output is unbounded. Fig. 3(c) shows a bounded input resulting in a bounded output. The trajectory is the result of $|{}^\mathrm{a}\mathbf{p}_\mathrm{h}(t_0)| = 150$ mm, $\beta_\mathrm{a} = 12.7°$, and $\dot{\gamma}_\mathrm{a} = 1.8°$/s. In this case the UHMD stays in an orbit with $\gamma = 0.252$ for all future time and the output is bounded. Note that the components ${}^\mathrm{a}p_{\mathrm{h}_x}$, ${}^\mathrm{a}p_{\mathrm{h}_y}$, and ${}^\mathrm{a}p_{\mathrm{h}_z}$ vary periodically and are uniformly bounded, and consequently the UHMD will stay in this closed orbit for all future time. *Please See supplementary multimedia.*

C. Input-Output Gain Characterization

To gain more insight into the input-output boundedness of the UHMD, actuation inputs (f_a, β_a, $|{}^\mathrm{a}\mathbf{p}_\mathrm{h}(t_0)|$, $\dot{\gamma}_\mathrm{a}$) are varied and γ is determined. The inputs are analyzed with respect to f_a, which determines the speed of the UHMD. The position vector ${}^\mathrm{a}\mathbf{p}_{\mathrm{h}_z}$ directly affects the magnetic field strength. The pitch angle β_a is varied since it determines the balance between the upward force and the forward motion of the UHMD. For each frequency the pitch, distance, and yaw speed leading to the lowest gain are determined, then β_a, $|{}^\mathrm{a}\mathbf{p}_\mathrm{h}(t_0)|$, $\dot{\gamma}_\mathrm{a}$ are used as inputs for the next frequency.

Fig. 4 shows that there are sets for each input (f_a, β_a, $|{}^\mathrm{a}\mathbf{p}_\mathrm{h}(t_0)|$, $\dot{\gamma}_\mathrm{a}$) resulting in a bounded output. For $\gamma < 1$, the output of the UHMD is bounded (stays in a periodic orbit). The pitch angle, β_a, has to decrease when the frequency increases to keep $\gamma < 1$, as shown in Fig. 4(a). Note that associated with an increase in the frequency is an increase in the speed, and this implies that if the speed of the UHMD, $\mathbf{v}_\mathrm{h}$, is required to increase, then β_a should be decreased. Furthermore, the numerical results show that at lower actuation frequencies the system stays bounded for a larger range of pitch angles than at high actuation frequencies. This property holds for the initial distance (Figs. 4(b)). In general, the gain at lower frequencies is lower, suggesting that low actuation frequencies are favoured (Figs. 4(a)-4(c)). In contrast to the pitch angle, to maintain $\gamma < 1$ for relatively high actuation frequency the yaw speed must be increased (Figs. 4(c)). The numerical results show sets of inputs leading to $0 < \gamma < 1$. Most likely, the reason for the bounded behavior is attributed to dynamic self-compensation through the RPM-UHMD-gap.

III. Experimental Input-Output Boundedness

A cylindrical magnet (NdFeB Grade-N45) with radius of 17.5 mm, height of 20.0 mm, magnetic moment of $\mathrm{M}_\mathrm{a} = 18.89$ A·m^2 is attached to a Maxon 18 V brushless DC motor. The motor is attached to a KUKA 6-DOF manipulator (KUKA KR-10 1100-2, KUKA, Augsburg, Germany). The

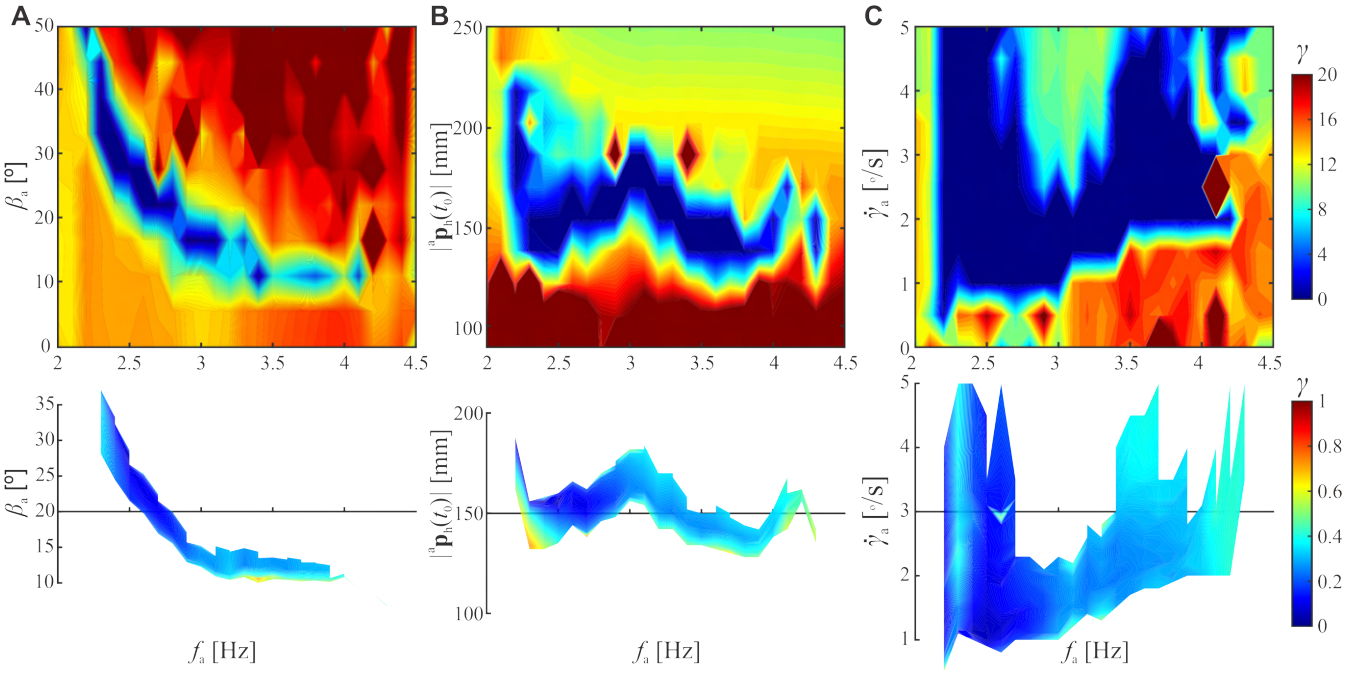

Fig. 4. The input-output gain of an untethered helical magnetic device is calculated during motion along circular trajectories for the inputs f_a, β_a, $|^a\mathbf{p}_h(t_0)|$, and $\dot{\gamma}_a$, and its gain γ is calculated for each output. There exist sets of inputs that result in a bounded output. (A)-(C) Top: Low resolution gain γ results of a wide input set for each input. (A)-(C) Bottom: High resolution gain γ results of input sets which lead to a bound on the output.

UHMD has a cylindrical magnetic head (NdFeB Grade-N52), with a magnetic moment $\mathbf{m}_h = 6.23 \times 10^{-4}$ A·m^2, head size of 1 mm and a helical body (Fig. 1). The helix has a length, outer diameter and pitch of 11.7 mm, 0.94 mm, 2.59 mm, respectively. Silicone oil (Carl Roth Gmbh Co. Kg, Karlsruhe, Germany), with viscosity of 1 Pa·s and density of 971 kg·m^{-3}, is contained inside 200 × 80 × 80 mm^3 plexiglass container. The UHMD is tracked with two FLIR Blackfly cameras (Teledyne FLIR LLC, Willsonville, Oregon) at 30 frames-per-second. The RPM is moved in straight runs with length of 160 mm. The UHMD is actuated at 3.5 Hz and in the $0° \leq \beta_a \leq 20°$, $91 \leq |^a\mathbf{p}_h(t_0)| \leq 112$ mm, $0.5 \leq \dot{\gamma}_a \leq 2°$/s ranges. Inputs are programmed in MATLAB (MathWorks, Inc., Natick, MA, USA) and exported to RoboDK (RoboDK Inc., Montreal, Canada).

To test the boundedness, open-loop experiments are conducted using a single RPM. The RPM is moved robotically at $f_a = 3.5$ Hz and $\dot{\gamma}_a = 0$. The RPM is initially placed such that its magnetic moment $\mathbf{M}_a$ is perpendicular to the long axis of the UHMD. The inputs β_a, $|^a\mathbf{p}_h(t_0)|$ and $\mathbf{v}_a$ are controlled and the path taken by the UHMD in open-loop motion control trials over time is depicted in Fig. 5. The UHMD is actuated at $f_a = 3.5$ Hz, $\beta_a = [0°, 13°, 20°]$, $|^a\mathbf{p}_h(t_0)| = 102$ mm, and RPM velocity $\mathbf{v}_a = 0.825$ mm/s. Setting $\beta_a = 20°$ results in a straight run trajectory, but with variations in height around 2 mm below the silicone oil-air interface. Similarly, setting $\beta_a = 13°$ results in a straight run with 3.5 mm below the silicone oil-air interface. Decreasing β_a further to 0°, causes the UHMD to fall downward under its own weight. The path of the falling UHMD (Fig. 5(c)) indicates that the output is unbounded, with $\gamma = 0.279$.

TABLE I

INPUTS OF THE RPM AND THE RESULTING EXPERIMENTALLY MEASURED OUTPUT y, RESULTING IN GAIN γ. THE INPUTS ARE FREQUENCY f_a, PITCH ANGLE β_a, INITIAL DISTANCE BETWEEN UHMD AND RPM $|^a\mathbf{p}_h(t_0)|$ AND VELOCITY OF THE RPM $\mathbf{v}_a$. THE GAIN IS CALCULATED WITH EQUATION (6) USING THE MEASURED UHMD'S TRAJECTORIES DURING OPEN-LOOP ACTUATION.

Inputs				**Output**	**Gain**
f_a [Hz]	β_a [°]	$\lvert^a\mathbf{p}_h(t_0)\rvert$ [mm]	$\mathbf{v}_a$ [mm/s]	$\lvert y\rvert$ [mm]	γ [–]
3.5	13	102	0.825	0.98	0.010
3.5	0	102	0.825	27.61	0.279
3.5	20	102	0.825	1.12	0.011
3.5	13	91.34	0.825	2.06	0.021
3.5	13	111.87	0.825	30.79	0.311
3.5	13	102	0.412	1.35	0.015
3.5	13	102	1.571	30.70	0.282

Although the input-output gain is less than 1, suggesting a bounded output, the UHMD is hindered by the bottom of the workspace resulting in lower gain. Again, $\beta_a = 20°$ results in a straight run, but the standard deviation of the average angle of attack β_h is greater than that of $\beta_a = 13°$. The trajectory shown in Fig. 5(a) shows wobbling locomotion, in contrast to the trajectory presented in Fig. 5(b). The larger standard deviation in combination with the wobbling locomotion suggest that the output is unbounded, despite the small gain $\gamma = 0.011$. This is confirmed by the smaller distance to the oil-air interface, suggesting that the UHMD is constrained by the surface tension. Fig. 5(b) shows that the output is bounded, the trajectory shows minimal wobbling and the UHMD stays below the surface with $\gamma = 0.010$.

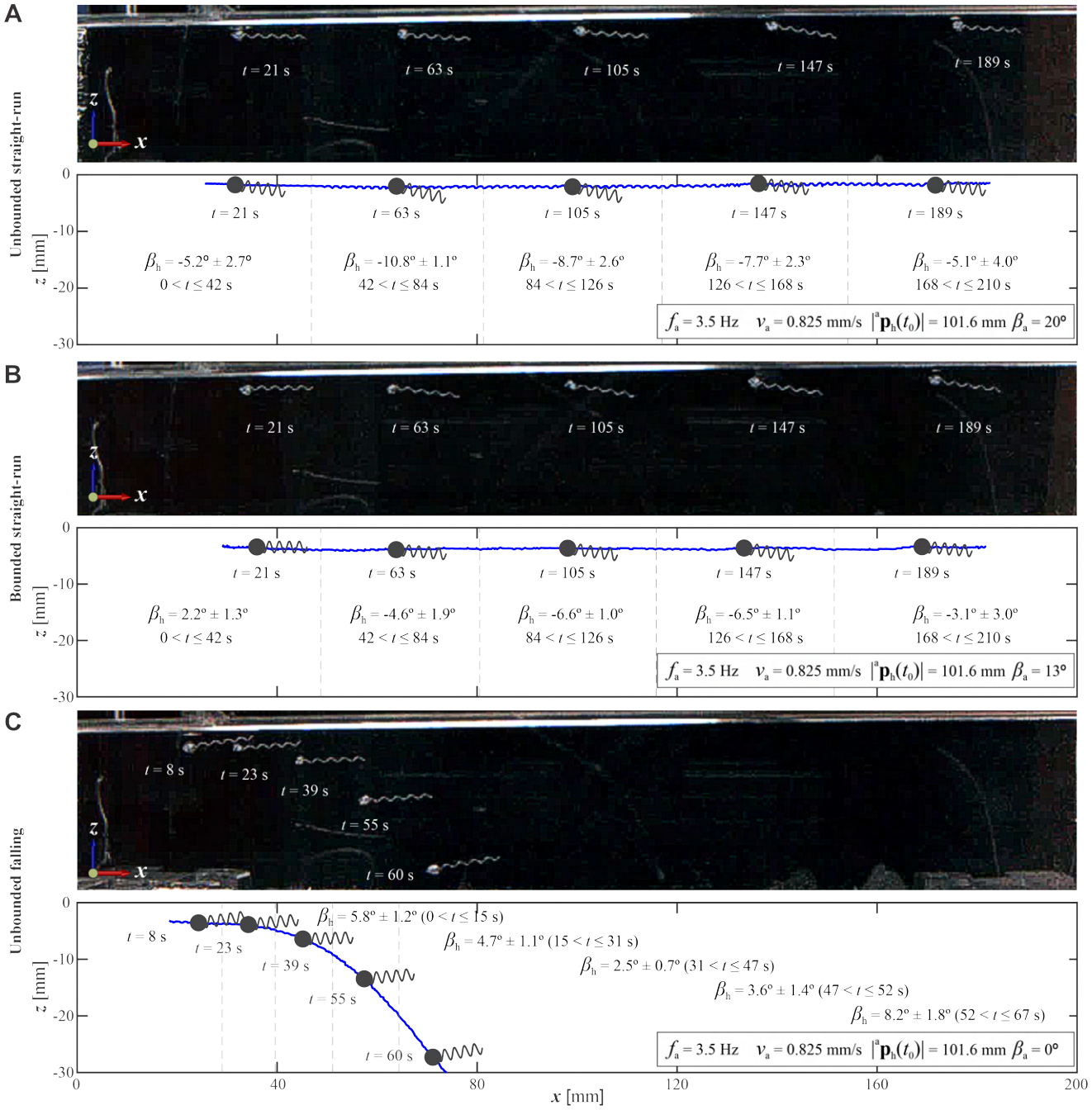

Fig. 5. Swimming path of an untethered helical magnetic device indicates its boundedness under three sets of bounded inputs. Error denotes standard deviation. (A) Straight-run with $\beta_a = 20°$. (B) Straight-run with $\beta_a = 13°$. (C) An unbounded behavior for $\beta_a = 0°$. *Please see supplementary multimedia.*

Note that the UHMD is swimming with a negative angle of attack (Fig. 5(b)). The UHMD is pointing downward, with an angle of attack $\beta_h \approx -6°$. This demonstrates that the propulsive thrust produced by a positive β_h is not responsible for the gravity compensation. Instead, the UHMD counteracts gravity by the magnetic force of the RPM, and this dynamic self-compensation enables swimming in the $\boldsymbol{xy}$-plane even with $\beta_h < 0°$. Table I presents the gain for different inputs and indicates that deviations from the inputs used in Fig. 5(b) results in an increase in γ. Decreasing β_a, increasing $|{}^a\mathbf{p}_h(t_0)|$, and increasing $\mathbf{v}_a$ result in a gain of ~ 0.3, indicating greater influence of the gravitational force. Note that the trajectory is truncated by the physical limit imposed by the limited vertical workspace. Increasing β_a, decreasing $|{}^a\mathbf{p}_h(t_0)|$, and decreasing $\mathbf{v}_a$ translated into a small increase in gain. However, these cases show a trajectory similar to Fig. 5(a), suggesting that their trajectory is obstructed by the workspace, so it is likely that these outputs are unbounded. Therefore, Table I suggests that unique sets do exist for each input (β_a, $|{}^a\mathbf{p}_h(t_0)|$, $\mathbf{v}_a$) for which the output stays bounded.

The experimental results suggest that dynamic self-compensation allows the UHMD to achieve straight runs

without feedback control. Let us consider the motion along the z-axis throughout one cycle of the RPM with respect to the UHMD. If we were able to keep the RPM and the UHMD in sync, the field-gradient pulling will tend to increase and decrease to a maximum and a minimum, respectively, two times per each rotation. The time-periodic switching between these values allows the UHMD to have bounded response and dynamic self-compensation. Only if the field-gradient pulling decreases as the RPM-UHMD-gap is decreased and becomes smaller than the action of gravity will it be possible for there to be a negative vertical displacement, mitigating the risk of unbounded attraction, and vice versa. As the RPM-UHMD-gap and the field-gradient pulling tend to increase simultaneously, magnetic coupling dominates over gravity and the UHMD reverses its motion along the vertical direction. This is the magnetic suspension strategy that enables the UHMD to periodically execute these vertical motion reversals, which leads to bounded behavior of the open-loop system. Consequently, an advantage of performing straight-runs without increasing the angle of attack with feedback control, is that the motion control design might not place strong demand on orientation localization.

IV. CONCLUSIONS

UHMDs can be actuated by a single RPM in such a way that their output is bounded under open-loop action with a bounded input. We show that there exist unique sets of inputs (frequency, pitch angle, lateral speed, and field strength) that yield bounded output. However, slight deviations from these sets result in undesirable attraction toward the RPM characterized by a finite escape time, or the UHMD would fall downward under its own weight with a monotonically increasing output. Our experimental results show the existence of such sets and demonstrate that UHMD can swim with arbitrary, or even negative, angle of attack and achieve dynamic self-compensation of gravitational forces. The angle of attack can be oriented so that it prevents the UHMD from being attracted to the RPM. The presented input-output boundedness of UHMDs will potentially enable predictable motion, even in the presence of sensory uncertainties during localization.

APPENDIX A

The viscous force and torque are given by [19]:

$$\begin{pmatrix}\mathbf{f}_{\text{visc}}\\ \boldsymbol{\tau}_{\text{visc}}\end{pmatrix} = -\left(\int_0^l \mathcal{M}\,\mathrm{d}s + \begin{bmatrix}\mathcal{A} & \mathcal{B}\\ \mathcal{B}^T & \mathcal{D}\end{bmatrix}\right)\begin{pmatrix}\mathbf{v}_{\text{h}}\\ \boldsymbol{\omega}_{\text{h}}\end{pmatrix}, \tag{7}$$

where $\mathcal{M} \in \mathbb{R}^{6\times6}$ is the the resistance matrix of the helix, $\mathcal{A} \in \mathbb{R}^{3\times3}$, $\mathcal{B} \in \mathbb{R}^{3\times3}$, and $\mathcal{D} \in \mathbb{R}^{3\times3}$ are the sub-matrices of the head's resistance matrix. The force, $\mathbf{f}_{\text{g}}$, is determined the volume, V, and the densities of the UHMD ρ_{r} and fluid ρ_{f}. The torque, $\boldsymbol{\tau}_{\text{g}}$, is given by the distance between the UHMD's center of mass (CoM) and volume (CoV), we have

$$\begin{pmatrix}\mathbf{f}_{\text{g}}\\ \boldsymbol{\tau}_{\text{g}}\end{pmatrix} = \begin{pmatrix}V(\rho_{\text{r}}-\rho_{\text{f}})\mathbf{R}_{\text{Lab}}^T\boldsymbol{g}\\ (\mathbf{r}_{\text{CoV}}-\mathbf{r}_{\text{CoM}})\times\mathbf{f}_{\text{g}}\end{pmatrix}. \tag{8}$$

The rotation matrix $\mathbf{R}_{\text{Lab}}^T \in \mathbb{R}^{3\times3}$ is added to correct for the rotation of the UHMD, $\mathbf{R}_{\text{Lab}} = \mathbf{R}_z(\gamma_{\text{h}})\mathbf{R}_y(\beta_{\text{h}})\mathbf{R}_x(\alpha_{\text{h}})$, where $\mathbf{R}_x(\alpha_{\text{h}})$ is the rotation matrix of the angle of the UHMD α_{h} about the x-axis. The magnetic field $\mathbf{B}({}^{\text{a}}\mathbf{p}_{\text{h}})$ is

$$\mathbf{B}({}^{\text{a}}\mathbf{p}_{\text{h}}) = \frac{\mu_0}{4\pi||{}^{\text{a}}\mathbf{p}_{\text{h}}||^3}(3\,{}^{\text{a}}\hat{\mathbf{p}}_{\text{h}}\,{}^{\text{a}}\hat{\mathbf{p}}_{\text{h}}^{\text{T}} - \mathbb{I})\mathbf{M}_{\text{a}}. \tag{9}$$

Here μ_0 is the permeability of free space and $\mathbb{I} \in \mathbb{R}^{3\times3}$ is the identity matrix.

REFERENCES

[1] T. W. R. Fountain, Prem V. Kailat, and J. J. Abbott, "Wireless control of magnetic helical microrobots using a rotating-permanent-magnet manipulator," in *Proc. IEEE Int. Conf. Robot. Autom.*, 2011, pp. 576–581.

[2] B. J. Nelson, I. K. Kaliakatsos, and J. J. Abbott, "Microrobots for minimally invasive medicine," *Annu. Rev. Biomed. Eng.*, vol. 12, pp. 55–85, 2010.

[3] M. Sitti, H. Ceylan, W. Hu, J. Giltinan, M. Turan, S. Yim, and E. Diller, "Biomedical applications of untethered mobile milli/microrobots," *Proc. IEEE*, vol. 103, no. 2, pp. 205-224, 2015.

[4] J. J. Abbott, K. E. Peyer, M. C. Lagomarsino, L. Zhang, L. Dong, I. K. Kaliakatsos, and B. J. Nelson, "How should microrobots swim?," *Int. J. Robot. Res.* vol. 28, no. 11–12, pp. 1434–47, 2009.

[5] A. W. Mahoney, J. C. Sarrazin, E. Bamberg, and J. J. Abbott, "Velocity control with gravity compensation for magnetic helical microswimmers," *Adv. Robot.*, vol. 25, no. 8, pp. 1007–1028, 2011.

[6] R. Venezian and I. S. M. Khalil, "Understanding robustness of magnetically driven helical propulsion in viscous fluids using sensitivity analysis," *Adv. Theory Simul.*, vol. 5, no. 4, pp. 2100519, 2022.

[7] T. Xu, G. Hwang, N. Andreff, and S. Régnier, "Planar path following of 3-D steering scaled-up helical microswimmers," *IEEE Trans. Robot.*, vol. 31, no. 1, pp. 117-127, 2015.

[8] J. Leclerc, H. Zhao, D. Bao, and A. T. Becker, "In Vitro design investigation of a rotating helical magnetic swimmer for combined 3-D navigation and blood clot removal," *IEEE Trans. Robot.*, vol. 36, no. 3, pp.975-982, 2020.

[9] J. J. Abbott, E. Diller, and A. J. Petruska, "Magnetic methods in robotics," *Annu. Rev. Control, Robot., Auton. Syst.*, vol. 3, pp. 57-90, 2020.

[10] A. Hosney, J. Abdalla, I. S Amin, N. Hamdi, and I. S. M. Khalil, "In vitro validation of clearing clogged vessels using microrobots," in *Proc. IEEE int. Conf. Biomed. Robot. Biomech.*, 2016, pp. 272–277.

[11] A. W. Mahoney and J. J. Abbott, "Generating rotating magnetic fields with a single permanent magnet for propulsion of untethered magnetic devices in a lumen," *IEEE Trans. Robot.*, vol. 30, no. 2, pp. 411–420, 2014.

[12] A. W. Mahoney and J. J. Abbott, "Control of untethered magnetically actuated tools with localization uncertainty using a rotating permanent magnet," in *Proc. IEEE int. Conf. Biomed. Robot. Biomech.*, 2012, pp. 1632–1637.

[13] Q. Wang, L. Yang, J. Yu, P. W. Y. Chiu, Y.-P. Zheng, and L. Zhang, "Real-Time magnetic navigation of a rotating colloidal microswarm under ultrasound guidance," *IEEE Trans. Biomed. Eng.*, vol. 67, no. 12, pp. 3403-3412, 2020.

[14] C. Di Natali, M. Beccani, and P. Valdastri, "Real-Time pose detection for magnetic medical devices," *IEEE Trans. Magn.*, vol. 49, no. 7, pp. 3524–3527, 2013.

[15] K. I. N. A. Middelhoek, V. Magdanz, L. Abelmann, and I. S. M. Khalil, "Drug-Loaded IRONSperm clusters: modeling, wireless actuation, and ultrasound imaging," *Biomed. Mater.*, vol. 17, no. 6, pp. 065001, 2022.

[16] S. Pane, G. Faoro, E. Sinibaldi, V. Iacovacci, and A. Menciassi, "Ultrasound acoustic phase analysis enables robotic visual-servoing of magnetic microrobots," *IEEE Trans. Robot.*, vol. 38, no. 3, pp. 1571-1582, 2022.

[17] H. K. Khalil, *Nonlinear systems*, 3rd ed. New Jersey, USA: Prentice Hall, 2002.

[18] Z.-P. Jiang, I. M. Y. Mareels, and Y. Wang, "A Lyapunov formulation of the nonlinear small-gain theorem for interconnected ISS systems," *Autom.*, vol. 32, no. 8, pp. 1211–1215, 1996.

[19] A. F. Tabak and S. Yesilyurt, "Improved kinematic models for two-link helical micro/nanoswimmers," *IEEE Trans. Robot.*, vol. 30, no. 1, pp. 14-25, 2014.